Please cite the Published Version

Gulten, G, Yaylali, B, Yesilyurt, M, Totik, Y, Kulczyk-Malecka, J , Kelly, P and Efeoglu, I (2025) Effect of transition metals (Nb, Ta, and V) doping on the high-temperature mechanical and tribological properties of CrYN coatings. Surface and Coatings Technology, 515. 132633 ISSN 0257-8972

DOI: https://doi.org/10.1016/j.surfcoat.2025.132633

Publisher: Elsevier

Version: Accepted Version

Downloaded from: https://e-space.mmu.ac.uk/641927/

Usage rights: Creative Commons: Attribution 4.0

Additional Information: This is an author accepted manuscript of an article published in Surface and Coatings Technology, by Elsevier. This version is deposited with a Creative Commons Attribution 4.0 licence [https://creativecommons.org/licenses/by/4.0/], in accordance with Man Met's Research Publications Policy. The version of record can be found on the publisher's website.

Data Access Statement: Data will be made available on request.

Enquiries:

If you have questions about this document, contact openresearch@mmu.ac.uk. Please include the URL of the record in e-space. If you believe that your, or a third party's rights have been compromised through this document please see our Take Down policy (available from https://www.mmu.ac.uk/library/using-the-library/policies-and-guidelines)

Effect of Transition Metals (Nb, Ta, and V) Doping on the High-Temperature Mechanical and Tribological Properties of Cryn Coatings

- Gokhan Gulten¹, Banu Yaylali¹, Mustafa Yesilyurt¹ Yasar Totik¹, Justyna Kulczyk-Malecka²,
 Peter Kelly², Ihsan Efeoglu^{1*}
- ¹Faculty of Engineering, Department of Mechanical Engineering, Atatürk University, 25240
- 6 Erzurum, Türkiye

1

2

10

- ² Surface Engineering Group, Manchester Metropolitan University, Manchester M1 5GD, UK
- 8 *Corresponding author.
- 9 E-mail address: <u>iefeoğlu@atauni.edu.tr</u> (Ihsan Efeoglu)

Abstract

- 11 This study focused on developing a high-temperature tribological coating for AISI 316L
- stainless steel. CrYN coatings doped with transition metals such as niobium, tantalum, and
- vanadium (Me-CrYN) were deposited using a closed-field unbalanced magnetron sputtering
- 14 (CFUBMS) system. In a previous study, the Taguchi L9 orthogonal array design was employed
- to optimize the deposition parameters based on tribological performance under dry sliding
- 16 conditions at room temperature. Among the nine experimental runs, the three coatings
- exhibiting the lowest friction coefficients and highest wear resistance were selected for high-
- temperature tribological testing. In the present work, these three optimized Me-CrYN coatings
- 19 were systematically evaluated for their tribological and adhesion properties at elevated
- 20 temperatures. High-temperature tribological performance was assessed using a pin-on-disc
- 21 tribometer in ambient air at 450 °C, 550 °C, and 650 °C, with particular attention given to their
- 22 frictional behavior. Additionally, adhesion strength was evaluated at room temperature via
- 23 scratch testing, both on the as-deposited coatings and those subjected to high-temperature
- 24 tribological testing at 450 °C, 550 °C, and 650 °C. The results demonstrate that the Me-CrYN
- coatings maintain tribomechanical stability at elevated temperatures, with hardness values
- ranging from 8.8 to 15.3 GPa. Nb-doped coatings exhibited a reduction in friction from ~0.55
- 27 at room temperature to ~ 0.30 at 650 °C ($\approx 45\%$ decrease), while Ta-doped coatings maintained
- stable values around 0.40 across all temperatures (<5% variation). In contrast, V-doped coatings
- showed an initial rise from ~ 0.13 at room temperature to ~ 0.30 at 450 °C ($\approx 115\%$ increase), but
- 30 then decreased to ~ 0.10 at 550 °C ($\approx 25\%$ below RT) and ~ 0.12 at 650 °C ($\approx 10\%$ below RT).
- 31 Adhesion strength was preserved after thermal exposure, supporting their potential for high-
- 32 temperature applications.
- 33 **Keywords:** Magnetron sputtering, AISI 316L, Me-doped CrYN, high-temperature tribological
- 34 testing, high-temperature adhesion

1. Introduction

- 36 Austenitic stainless steels, particularly AISI 316L, are extensively used across diverse industrial
- sectors, including petrochemical processing, power generation, and biomedical engineering,
- due to their excellent corrosion resistance, mechanical strength at room temperature, and good
- 39 formability [1–3]. Despite these advantages, their relatively low hardness and susceptibility to

friction and wear-related failures significantly limit their performance, especially under elevated temperature conditions [4].

42

43

44

45

46

47

48

49

50

51

52

53

54

55

56

57

58

59

60

61

62

63

64

65

66

67

68

69

70

71

72

In applications such as heat exchangers, orthopedic implants, and marine systems, prolonged exposure to friction and reactive environments often leads to the formation of abrasive debris and surface oxides, which accelerate material degradation. These challenges highlight the necessity of enhancing the surface properties of stainless steels to extend their functional lifespan. Among various surface engineering strategies, thermal and tribological coatings are considered effective in minimizing friction, wear, and oxidation, particularly in aggressive service environments [5–8]. In this respect, transition metal nitrides such as TiN, CrN, NbN, ZrN, and TaN have received considerable attention due to their outstanding hardness, wear resistance, and stability at elevated temperatures, making them ideal for applications requiring enhanced tribological performance under severe mechanical and chemical stresses [9-13]. However, despite their excellent properties, monolayer nitride coatings often suffer from certain limitations such as intrinsic brittleness, poor oxidation resistance at very high temperatures, and limited adhesion when applied to substrates like austenitic stainless steels. For instance, while TiN provides high hardness, its thermal stability and wear resistance tend to deteriorate beyond 500 °C due to phase transformations or oxide scale formation. Furthermore, the lack of compositional complexity in single-transition-metal nitrides restricts their ability to accommodate thermal stresses and maintain mechanical integrity under cyclic or extreme loading conditions. To overcome these limitations, researchers have increasingly focused on binary, ternary, quaternary, and even quinary nitride systems, where alloying with multiple transition metals enhances high-temperature behavior by improving solid solution hardening, defect tolerance, and oxidation resistance. In this context, the co-addition of yttrium (Y) and selected transition metals (Me = Nb, Ta, or V) offers a promising route for performance enhancement. Y, due to its large ionic radius and strong affinity for oxygen, preferentially segregates to grain boundaries, refining the microstructure, increasing compressive residual stresses, and significantly retarding oxygen diffusion—thereby improving oxidation resistance and thermal stability at elevated temperatures. The additional transition metals were selected for their complementary effects: Nb and Ta, as refractory elements, enhance hardness retention, solid-solution strengthening, and high-temperature mechanical stability, whereas V is wellknown for its self-lubricating behavior at elevated temperatures via the formation of low-shearstrength vanadium oxides (e.g., V2O5), which reduce the coefficient of friction and improve wear resistance. While each of these elements has been individually investigated in various

- nitride systems, there is a distinct lack of high-temperature tribological studies on CrYN coatings specifically co-doped with Y and Nb, Ta, or V. The combination of Y for grain boundary engineering and thermal stability, with dopant-specific mechanical reinforcement or friction reduction effects, is expected to produce a quaternary nitride matrix (Cr–Y–Me–N) with synergistic benefits [14–18].
- In the present study, three Me (Nb, Ta, and V)-doped CrYN coatings that were previously developed and optimized in earlier work [19,20] using the Taguchi L9 orthogonal design based on their room temperature tribological performance were subjected to high-temperature tribological testing at 450 °C, 550 °C, and 650 °C to evaluate their adhesion and friction behavior under thermal loading.

2. Materials and Methods

83

84

85

86

87

88

89

90

91

92

93

94

95

96

97

98

99

100

101

102

103

104

105

Me-doped CrYN coatings were deposited on AISI 316L, glass, and Si (111) substrates using reactive closed-field unbalanced magnetron sputtering (CFUBMS) in a Teer Coating Ltd. UDP550 coating system. AISI 316L steel was used as the primary substrate for adhesion and tribological testing, since this is the technologically relevant material for high-temperature applications. Si(100) wafers were used for cross-sectional SEM analysis and thickness evaluation. Due to their brittle nature, Si substrates readily develop radial cracks upon fracturing, which allows for clearer imaging of the coating architecture. This approach is widely adopted in the thin film literature to obtain high-quality cross-sectional SEM images of PVD coatings. Glass substrates were employed only for supplementary observations, primarily to check coating uniformity and surface appearance. The deposition process was optimized using a Taguchi L9 orthogonal array to investigate the influence of different sputtering parameters, including CrY target current, deposition pressure, and the duty cycle of the pulsed-DC power applied to the CrY targets. These three parameters were intentionally selected as variables due to their significant influence on coating growth dynamics: (i) CrY target current directly controls the sputtering rate of Cr and Y atoms, thereby affecting film thickness, composition, and microstructure; (ii) deposition pressure influences the mean free path and kinetic energy of sputtered species, which in turn modifies adatom mobility, nucleation behavior, and coating density; and (iii) duty cycle, defined as the percentage of each pulse period during which power is applied to the CrY targets in pulsed-DC mode, determines ionization dynamics, heat input to the target, and plasma-substrate interaction, thus affecting residual stress, grain refinement, and defect density. Optimization was based on mechanical and tribological test results obtained at room temperature[19,20]. Microstructural analyses were performed on coatings deposited on

Si (111) substrates to evaluate surface morphology and layer architecture. The deposition parameters listed in Table 1 were validated through coatings deposited under the optimal conditions determined by the Taguchi analysis. Fig. 1 illustrates the magnetron configuration for Nb, Ta, and V doping, as well as the schematic representation of the resulting coating architecture. Prior to deposition, AISI 316L substrates were ultrasonically cleaned and mechanically ground using 400, 600, 800, and 1200 grit SiC abrasive papers to achieve a fine surface finish with an average roughness of approximately $0.02~\mu m$ (Ra), ensuring proper adhesion and coating uniformity.

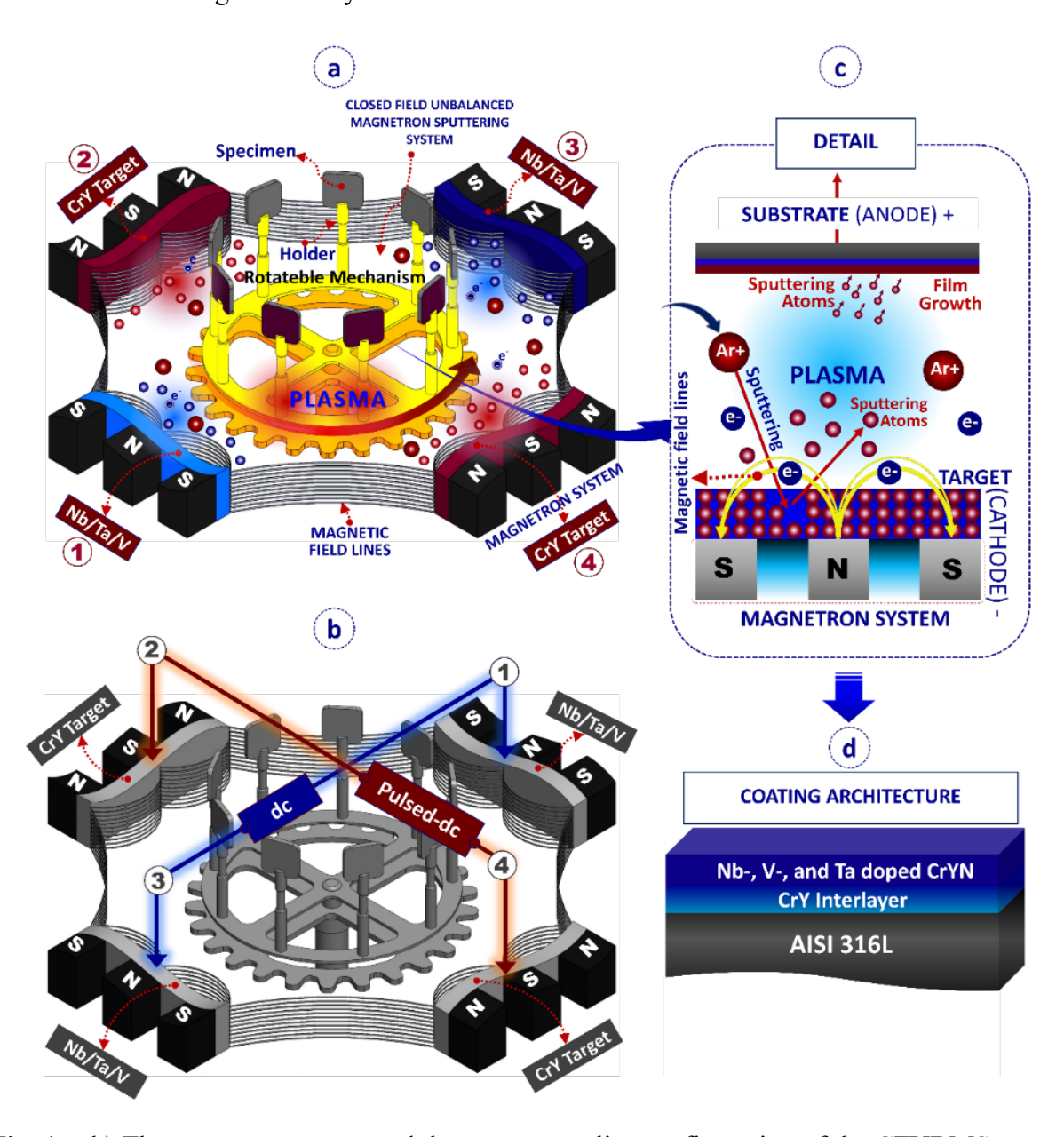


Fig. 1 a, b) The target magnetron and the power supplies configuration of the CFUBMS deposition system c) sputtering detail and d) structural design of Nb-, Ta-, and V-doped CrYN coatings detail [19, 20]

Table 1. Deposition parameters levels and variables of Nb-, Ta-, and V-doped CrYN coatings [19-21]

The variable Parameters	Level 1	Level 2	Level 3
CrY Target Current (A)	1.5	2	1
Deposition Pressure (Pa)	0.35	0.25	0.15
Duty Cycle (%)	50	30	15
The Constant Parameters			
CrY Interlayer	CrY: 2A (10 min)		
Me-doped CrYN Layer	Nb: 2A, Ta: 2A V:2A (90 min)		

No. 2A, Ta: 2A V:2A (90 min)

No. 2A, Ta: 2A V:2A (90 min)

No. 2A, Ta: 2A V:2A (90 min)

6

CrY: 0.05A, Me (Nb, Ta or V):

0.05A 30 min.

Substrate Bias (-V)

50

119 120

121

122

123

124

125

126

127

128

129

130

131

132

133

134

135

136

137

138

139

140

 Table 2. Experimental runs for Nb-, Ta-, and V-doped CrYN coatings [19-21]

	Duty Cycle	Deposition	CrY Target
	(%)	Pressure (Pa)	Current (A)
HT-1	50	0.35	1.5
HT-2	30	0.25	2
HT-3	15	0.15	1

During the coating process, Me-doped CrYN films were deposited using a combination of two CrY targets (99.95% pure) and one additional transition metal target (99.95% pure) (Nb, Ta, or V), depending on the specific film composition. The CrY targets consisted of 97 atomic percent chromium and 3 atomic percent yttrium, with all targets having a purity of 99.95%. Power was supplied to the CrY targets through a pulsed-DC unit (Advanced Energy Pinnacle Plus), while a separate DC source (Advanced Energy Pinnacle) powered the Nb, Ta, and V targets. Gas flow during deposition was carefully regulated using mass flow controllers to maintain stable chamber pressure. Nitrogen flow was fixed at 6 sccm across all coating runs, whereas argon flow varied between 10 and 20 sccm depending on the desired deposition pressure (see Table 2). Substrates were placed on a rotating holder that enabled one-degree oscillation in front of the targets, ensuring uniform film formation. The distance between the target and substrate was fixed at 70 mm. Before coating, the substrates were subjected to ion cleaning for 30 minutes in an argon plasma atmosphere using a -800 V DC bias to remove surface impurities and improve interfacial bonding, while a low target current of 0.05 A was applied to both the CrY and Me (Nb, Ta, or V) targets to prevent sputtering during this cleaning stage. A CrY interlayer was subsequently applied for 10 minutes to further support adhesion by forming a graded interface between the metallic substrate and ceramic layer. The current supplied to the CrY targets during this stage was fixed at 2 A for all samples. Following this, the main CrYN coatings doped with Nb, Ta, or V were deposited over a duration of 90 minutes.

The deposited Me-doped CrYN coatings were analyzed using various characterization techniques to evaluate their structural, mechanical, and tribological properties. Microstructural analysis was performed using a Zeiss Sigma 300 Scanning Electron Microscope (SEM). The crystal structures of the deposited coatings were examined via X-ray diffraction (XRD) using a Rigaku DMax-2200 system with a Cu-K α radiation source ($\lambda = 1.5405$ Å) and scanned over the range of 30-100°. The nanohardness of the coatings was measured using an Anton Paar Step 500 nanohardness tester equipped with a Berkovich indenter, applying a 3 mN load at 25 randomly selected different points to ensure reliable data collection. The critical load values were assessed using a CSM Instruments scratch tester, applying a progressive loading rate of 100 N/min with a Rockwell-C diamond indenter (200 μm tip radius). To assess the tribological properties of the coatings, tests were initially performed at room temperature using a CSM tribometer operated under ambient air. The tests were conducted under a constant normal load of 1 N, at a sliding speed of 10 cm/s, using an Al₂O₃ ball with a diameter of 6.25 mm as the counterface material. Subsequent measurements at elevated temperatures of 450 °C, 550 °C, and 650 °C were performed using a CSM high-temperature tribometer designed for in situ testing under thermal conditions. These evaluations provided detailed insights into the frictional behavior and wear resistance of the CrYN coatings doped with Nb, Ta, and V under both standard and elevated-temperature operating conditions. To further investigate the effect of thermal exposure on interfacial bonding, adhesion tests were performed at room temperature on samples that had previously undergone tribological testing at the aforementioned elevated temperatures.

3. Results and discussions

141

142

143

144

145

146

147

148

149

150

151

152

153

154

155

156

157

158

159

160

161

162

163

164

165

166

167

168

169

170

171

172

173

The cross-sectional SEM images of Me-doped CrYN coatings (Me = Nb, Ta, V), deposited under comparable sputtering conditions for each experimental group (HT-1, HT-2, HT-3) as listed in Table 2, reveal notable differences in film thickness despite consistent deposition time, pressure, duty cycle, and CrY target current within each set, as shown in Fig. 2 [19,20]. Among the three dopants, Ta-doped CrYN coatings (HT-1, HT-2, HT-3) exhibit the highest thicknesses, followed by Nb-doped coatings, while V-doped films consistently show the lowest values. These variations can be attributed to the intrinsic sputtering characteristics of the dopant elements and their influence on plasma dynamics during deposition. Ta, being a high-mass refractory metal (atomic mass: 180.95 g/mol), may exhibit a relatively higher sputtering yield under ion bombardment, potentially leading to a denser plasma and increased deposition rates. In addition, its low volatility and high momentum transfer efficiency could reduce re-sputtering

effects, thereby facilitating more efficient film growth [22–24]. This is consistent with observations in Ta-doped transition metal nitride systems, where Ta incorporation has been associated with increased deposition rates and enhanced coating thickness. In contrast, Nb-doped CrYN coatings display intermediate thicknesses, which may be due to the moderate sputtering yield of Nb and its lower atomic mass (92.91 g/mol) compared to Ta [20,25,26]. While Nb likely supports reasonable deposition efficiency, its lower momentum transfer capability and reduced scattering cross-section could limit plasma densification, resulting in relatively thinner coatings. On the other hand, V-doped CrYN coatings exhibit the thinnest films among the three. This may be attributed to the lower atomic mass of vanadium (50.94 g/mol), its higher surface reactivity, and greater susceptibility to re-sputtering, which can diminish net film growth [19,27,28] . Furthermore, the higher volatility of V atoms may contribute to increased scattering and reduced sticking probability at the substrate surface, as observed in related systems. Overall, these findings suggest that even under fixed process parameters, the choice of dopant element can significantly influence the growth kinetics and resulting film thickness in CrYN-based coatings.

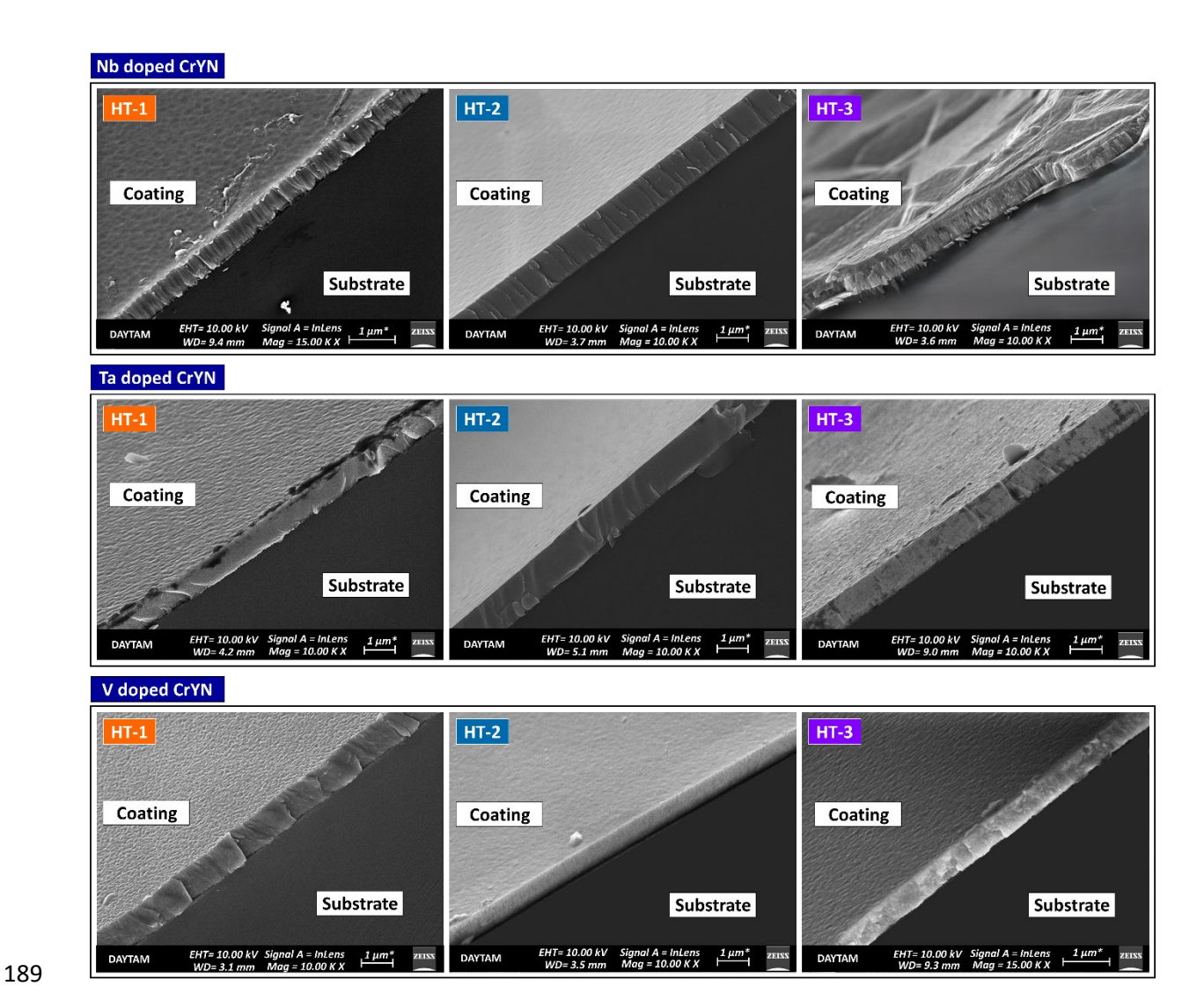


Fig 2. Cross-sectional SEM images of Nb-, Ta-, and V-doped CrYN coatings synthesized under three different optimized conditions: HT-1, HT-2, and HT-3 [19,20]

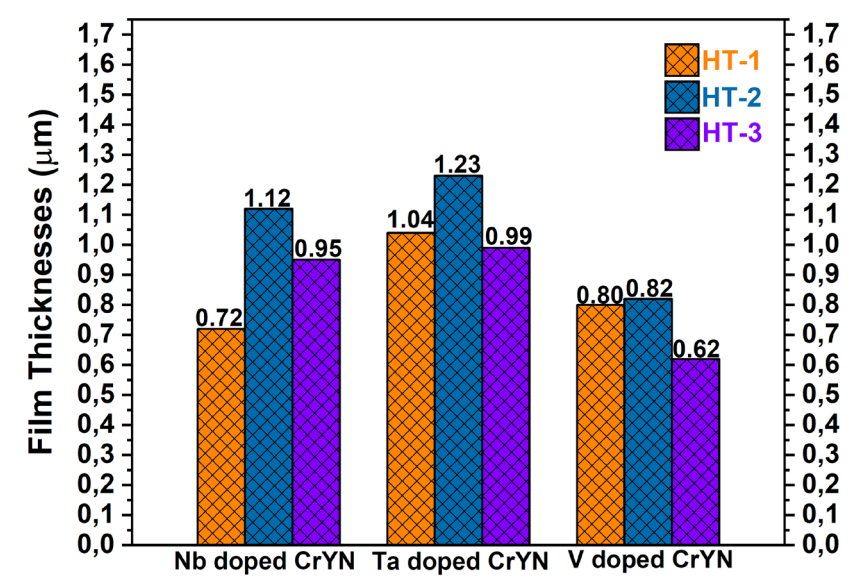


Fig 3. Film thickness of Nb-, Ta-, and V-doped CrYN coatings [19,20]

194	

196

197

198

199

200

201

202

203

204

205

206

207

208

209

210

211

212

213

214

215

		HT-1	HT-2	HT-3
at. %	Cr	39.90	55.29	31.25
	Y	0.76	0.76	0.61
	\mathbf{N}	16.06	15.04	17.82
	Nb	43.28	28.91	50.32

Table 4. Elemental composition of Ta-doped CrYN thin films

		HT-1	HT-2	HT-3
at. %	Cr	41.59	49.03	29.50
	Y	1.15	1.42	1.55
at. 70	\mathbf{N}	26.59	20.74	30.68
	Ta	30.67	28.81	38.27

Table 5. Elemental composition of V-doped CrYN thin films

		HT-1	HT-2	HT-3
at. %	Cr	33.71	49.67	32.18
	Y	0.60	0.63	0.56
at. 70	N	17.29	19.98	18.01
	V	48.40	29.72	49.24

A closer examination of film thicknesses, as presented in Fig. 3a, reveals that the highest values were consistently obtained under HT-2 deposition conditions for all three Me-doped CrYN coatings. These conditions correspond to the highest CrY target current applied among the experimental runs, as summarized in Table 2. This observation is consistent with our previous work, in which the influence of process parameters, particularly target current, on film growth dynamics was examined in detail [19,20]. Elemental analysis results given in Table 3-5 further support this finding, indicating that the atomic percentages of both Cr and Y increase with increasing CrY target current. This enrichment of the CrY-derived elements directly correlates with the enhanced film thicknesses observed in HT-2 coatings. The increase in Cr content, in particular, contributes significantly to the growth rate of the Me-doped CrYN films. Chromium is known to exhibit a relatively high sputtering yield under argon ion bombardment, with values reported around 0.7 atoms/ion at typical magnetron sputtering energies [23]. As the flux of Cr atoms to the substrate increases with higher target current, the probability of nucleation and subsequent film growth rises accordingly, leading to thicker coatings [29–31]. This finding aligns with previous studies showing that film deposition rates are strongly dependent on the availability of metal species with high sputtering yields, especially when their content dominates the coating matrix. In this context, the observed increase in Cr and Y concentrations at higher target currents could enhance the total material flux toward the substrate, thereby promoting the formation of denser and thicker films. The combined effect of increased Cr sputter flux and Y-induced refinement may account for the significant thickness enhancement under HT-2 conditions across all Me-doped compositions.

216

217

218

219

220

221

222

223

224

225

226

227

228

229

230

231

232

233

234

235

236

237

238

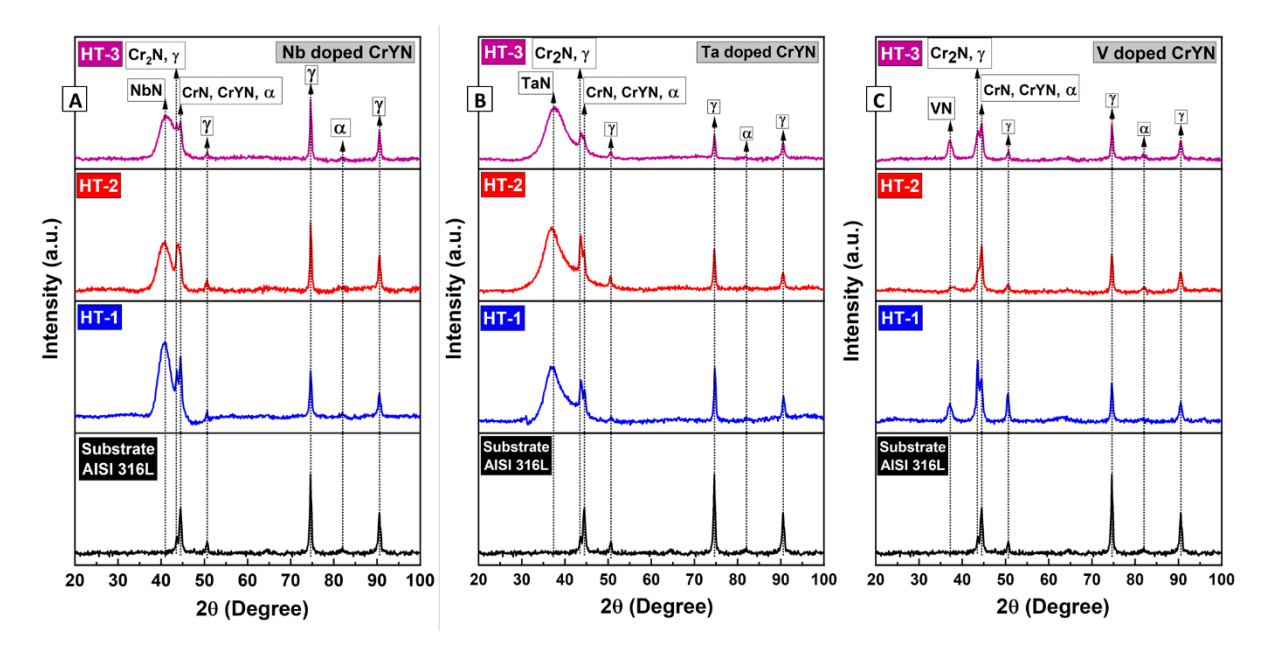


Fig. 4. XRD graphs of; a) Nb-doped CrYN coatings, b) Ta-doped CrYN coatings and c) V-doped CrYN coatings [19,20]

The XRD patterns of Me-doped CrYN coatings deposited on 316L substrates under different process parameters are presented in Fig. 4. All coatings exhibited a face-centered cubic (FCC) structure, with diffraction peaks corresponding to CrN and γ-Fe phases. A slight shift and broadening of the CrN peaks toward lower angles were observed, which can be attributed to compressive residual stresses induced during sputtering and lattice distortion resulting from the substitution of Cr3+ ions with larger Y3+ atoms. This behavior is consistent with Bragg's law and has been discussed in detail in our previous work [19,20,32]. Notably, the coatings produced under HT-2 conditions exhibited stronger and sharper diffraction peaks, suggesting enhanced crystallinity. This is likely due to the higher CrY target current (2 A) and optimal duty cycle (70%), which increases energy input and promote grain growth and preferred orientation. For Ta-doped CrYN coatings, similar peak shifting trends were noted, further confirming the influence of dopant atomic radius on lattice expansion and crystal structure. Although the nitrogen flow rate was fixed at 6 sccm for all depositions, elemental analysis (Fig. 3b) revealed that coatings deposited under HT2 consistently contained the lowest nitrogen content across all dopant types. This reduction can be linked to the increased metallic flux at higher target current, which suppresses nitrogen incorporation through competitive site occupation and surface re-sputtering mechanisms, as reported in high power PVD studies [33,34]. In contrast, the nitrogen content was higher in HT1 and HT3, likely due to lower Cr flux, longer nitrogen residence time, and favorable pressure conditions that enhance nitrogen retention.

239

240

241

242

243

244

245

246

247

248

249

250

251

252

253

254

255

256

257

The mechanical performance of the Me-doped CrYN coatings was evaluated using nanoindentation. To minimize substrate influence, indentation depth was limited to below 100 nm, corresponding to approximately 10% of the film thickness. The hardness values obtained via nanoindentation are presented in Fig. 5a, while the nanoindentation load-displacement curves are shown in Fig. 5b, 5c, and 5d. The highest hardness value measured for Nb-doped CrYN coatings was 15.3 ± 0.5 GPa under HT-2. In comparison, Ta-doped CrYN coatings exhibited relatively uniform hardness values across different runs, with the highest reaching 14.7 ± 0.5 GPa. For V-doped CrYN coatings, the maximum hardness obtained was 14.3 ± 0.5 GPa. These differences in hardness may be attributed to variations in microstructure, residual stress, and chemical bonding. The incorporation of Nb and Ta, both refractory elements, could contribute to grain refinement and enhanced solid solution strengthening [35]. Ta, in particular, is reported to improve high-temperature mechanical stability, which may explain the promising hardness and wear resistance observed in Ta-doped coatings [36,37]. In contrast, the slightly lower hardness values in V-doped films could be linked to the tendency of vanadium to reduce friction and wear, particularly under high-temperature conditions. Overall, these results suggest that transition metal doping plays a key role in tailoring the mechanical behavior of CrYN coatings for specific performance requirements.

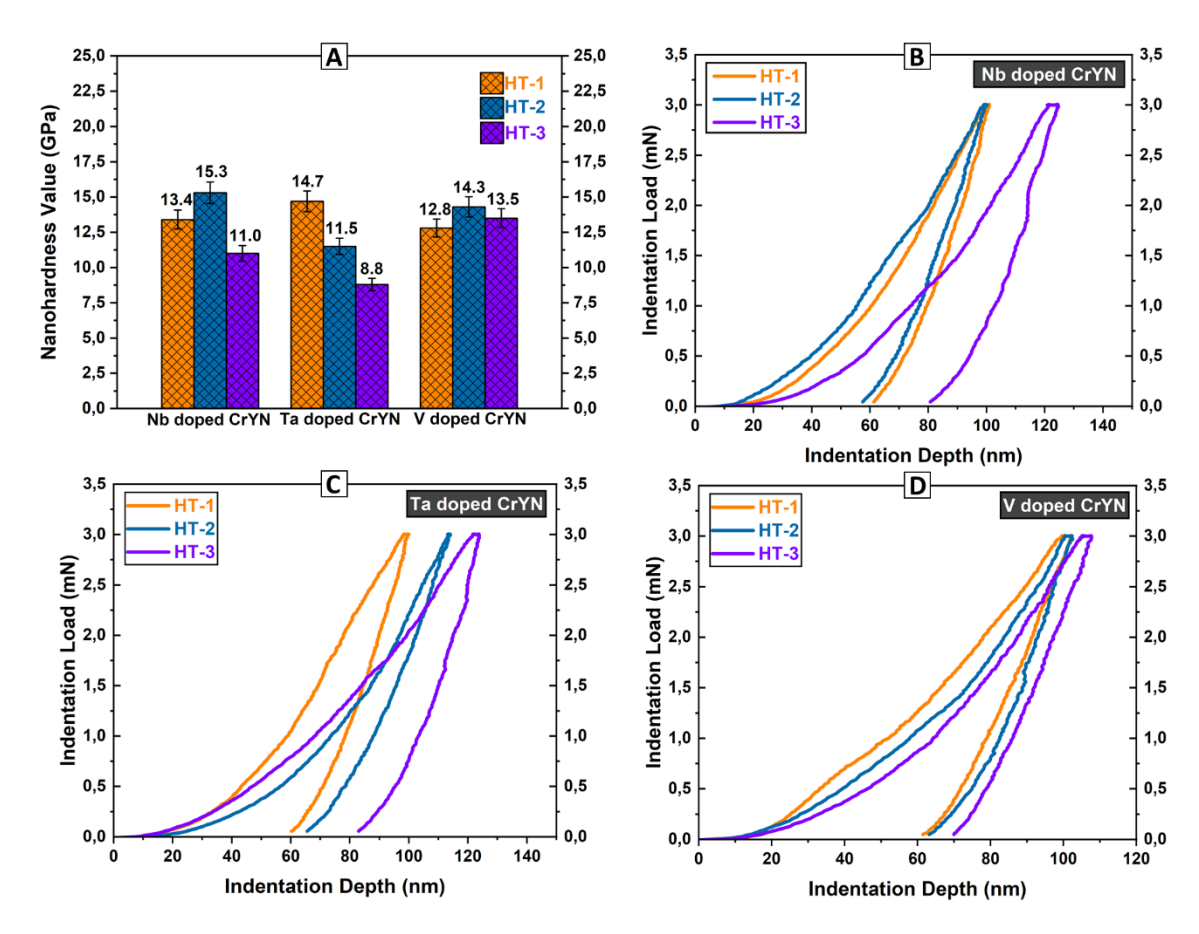


Fig. 5. a) Hardness values of Nb-, Ta-, and V-doped CrYN coatings, b) Nanoindentation curves of Nb-doped CrYN coatings, c) Nanoindentation curves of Ta-doped CrYN coatings, d) Nanoindentation curves of V-doped CrYN coatings [19,20]

Adhesion test results conducted at room temperature under a maximum load of 150N demonstrated that all Me-doped CrYN coatings retained their integrity without complete delamination, consistent with our previous findings [19]. Although progressive failure stages (Lc1, Lc2) could not be determined due to the lack of detailed imaging, typical failure modes such as conformal cracking, edge buckling, and localized delamination were observed across all samples. Among the three systems, V-doped coatings exhibited the least damage, suggesting higher interfacial toughness, followed by Ta- and Nb-doped films. These results reinforce earlier observations indicating strong adhesion performance of CrYN coatings, particularly those doped with vanadium, as illustrated in Fig. 6.



Fig. 6. Scratch test results (Room temperature) for Nb-, Ta-, and V-doped CrYN coatings



Fig. 7. Scratch test results (450°C, 550°C and 650°C) for Nb-doped CrYN coatings



Fig. 8. Scratch test results (450°C, 550°C and 650°C) for Ta-doped CrYN coatings

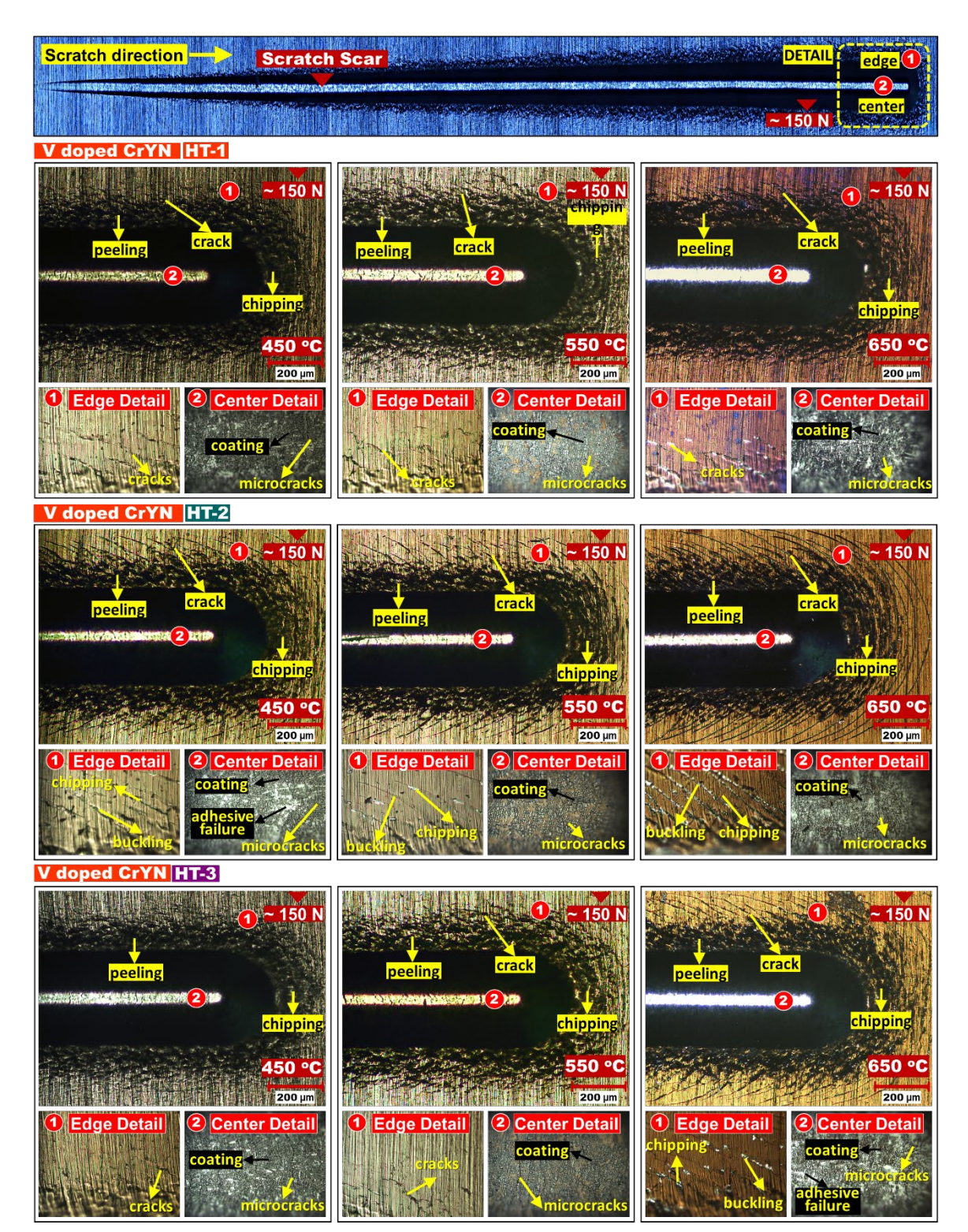


Fig. 9. Scratch test results (450°C, 550°C and 650°C) for V-doped CrYN coatings

The adhesion performance of Nb-, Ta-, and V-doped CrYN thin films subjected to annealing at 450 °C, 550 °C, and 650 °C is presented in Fig. 7, Fig. 8, and Fig. 9, respectively. Thermal treatments are known to affect coating adhesion through mechanisms such as interfacial diffusion, residual stress relaxation, or interface oxidation. While such effects can lead to either degradation or improvement in adhesion depending on the conditions, the scratch test results in

this study showed neither a decrease nor an improvement in adhesion after annealing at elevated temperatures, indicating that the coating maintained stable adhesion performance [38–40]. All CrYN-based coatings retained their structural integrity under the maximum applied load of 150 N, with no evidence of delamination or substrate exposure. These findings indicate strong thermal compatibility with the AISI 316L substrate and are consistent with previous reports emphasizing the excellent thermal and chemical stability of CrN-based systems, particularly when doped with refractory elements such as Nb, Ta, and V.

After annealing, distinct surface color changes were observed in all doped coatings. Because conventional θ –20 XRD analysis did not reveal crystalline oxide peaks, any oxidation—if present—is likely confined to nanometric and/or amorphous surface films below the detection limit of this technique. The bluish hue in Nb- and Ta-doped coatings and the brownish coloration in V-doped coatings are therefore interpreted as being consistent with thin-oxide interference/temper coloration rather than taken as definitive phase identification. While Nb and Ta oxides are typically transparent and capable of producing interference colors due to their high refractive index and low absorption, V oxides are generally more optically absorptive, leading to darker surface tones. Direct confirmation of oxide chemistry and thickness requires surface-sensitive methods such as X-ray photoelectron spectroscopy (XPS) or grazing-incidence XRD which will be addressed in future work. Importantly, the scratch test results indicate that any surface films formed after annealing are thin and non-deleterious to adhesion.

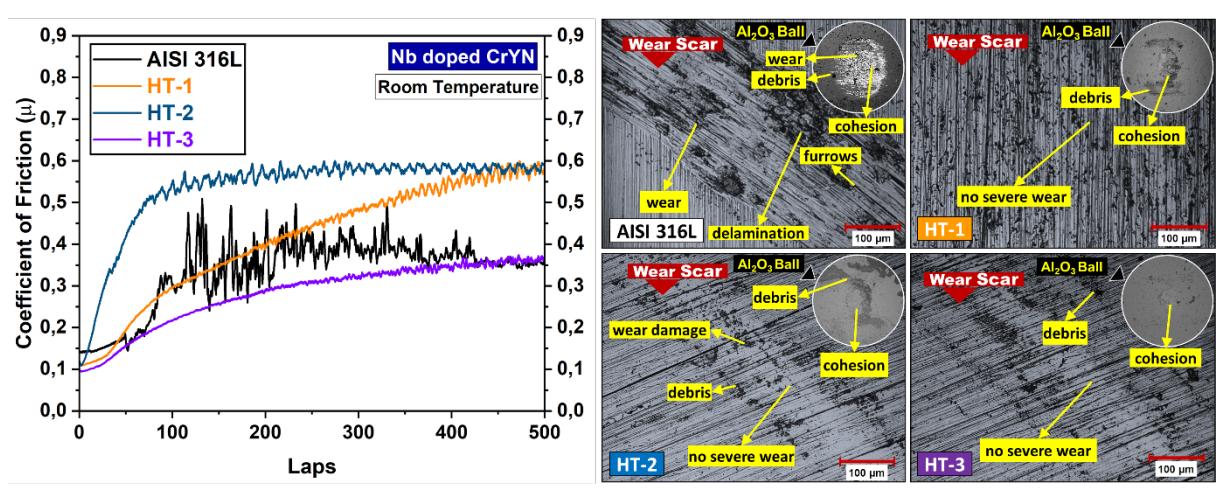


Fig 10. CoF values and optical images of the pin and worn coating surfaces for Nb-doped CrYN coatings [19].

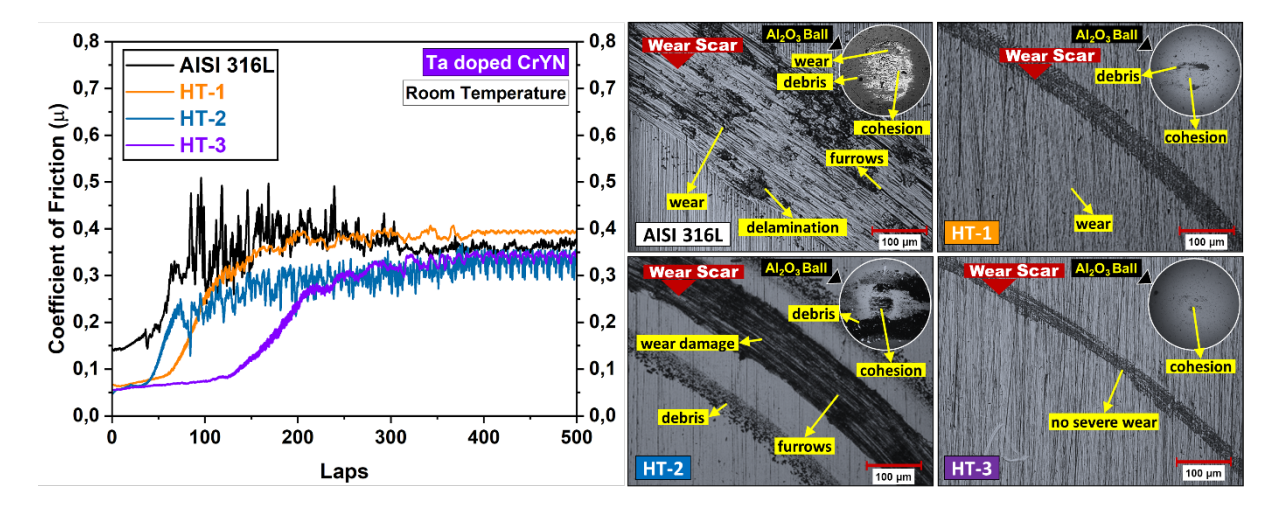


Fig 11. CoF values and optical images of the pin and worn coating surfaces for Ta-doped CrYN coatings [19].

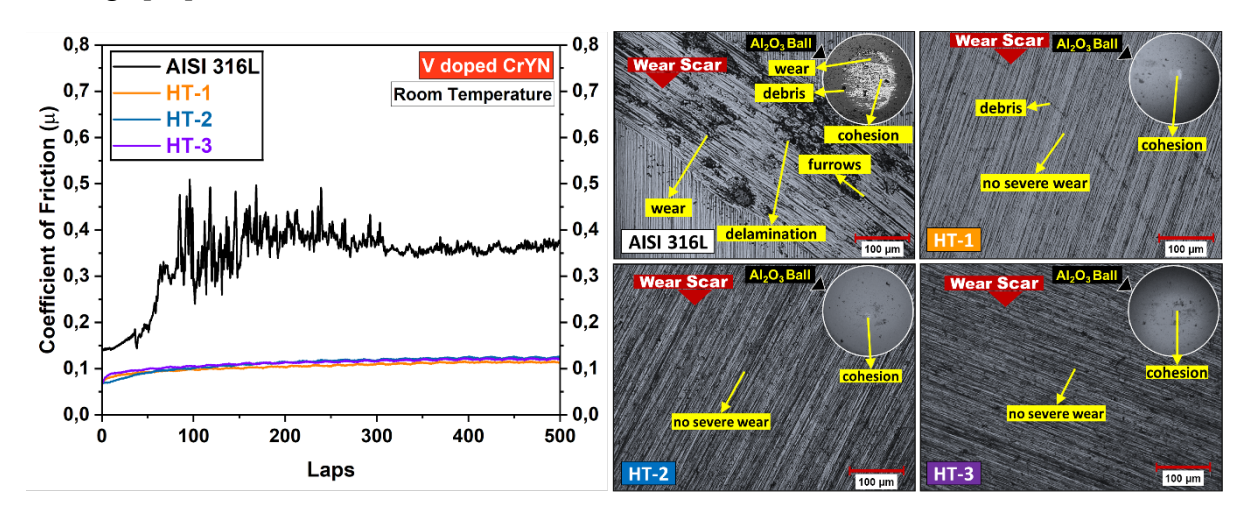


Fig 12. CoF values and optical images of the pin and worn coating surfaces for V-doped CrYN coatings [19].

High-temperature tribological properties of Me-doped CrYN coatings were examined using a CSM Instruments tribometer equipped with a high-temperature module. Three coatings (HT-1, HT-2, and HT-3), optimized in previous studies and deposited on 316L stainless steel substrates, were tested at 450 °C, 550 °C, and 650 °C (see Fig. 13, 14, and 15). Tests were performed sequentially at increasing temperatures, and a new Al₂O₃ ball was used for each cycle to ensure consistency.

The frictional behavior of Me-doped CrYN coatings was systematically evaluated at room temperature and after annealing at 450 °C, 550 °C, and 650 °C. Notably, Nb-doped coatings exhibited a consistent decrease in the coefficient of friction with increasing temperature. This may be attributed to surface smoothening, stress relaxation, or possible surface chemistry changes, although further analysis would be required to confirm the exact mechanisms. The trend was particularly evident for HT-1 and HT-2, where the coefficient of friction decreased

from approximately 0.55 at room temperature to below 0.30 after annealing at 650 °C. Ta-doped coatings showed moderate and stable friction values across all temperatures, with minimal fluctuation. The frictional response remained largely unaffected by thermal treatment, which may suggest a thermally stable surface structure. In contrast, V-doped coatings demonstrated a different behavior. While the coefficient of friction increased slightly after 450 °C, it gradually decreased at higher temperatures. This behavior might be related to changes in surface morphology or reduction of wear debris at elevated temperatures. Among all samples, HT-2 consistently exhibited the lowest and most stable friction values, indicating that its deposition parameters were effective in producing a dense and wear-resistant structure. These findings suggest that annealing at temperatures above 550 °C can improve the frictional performance of CrYN coatings, particularly in Nb-doped variants.

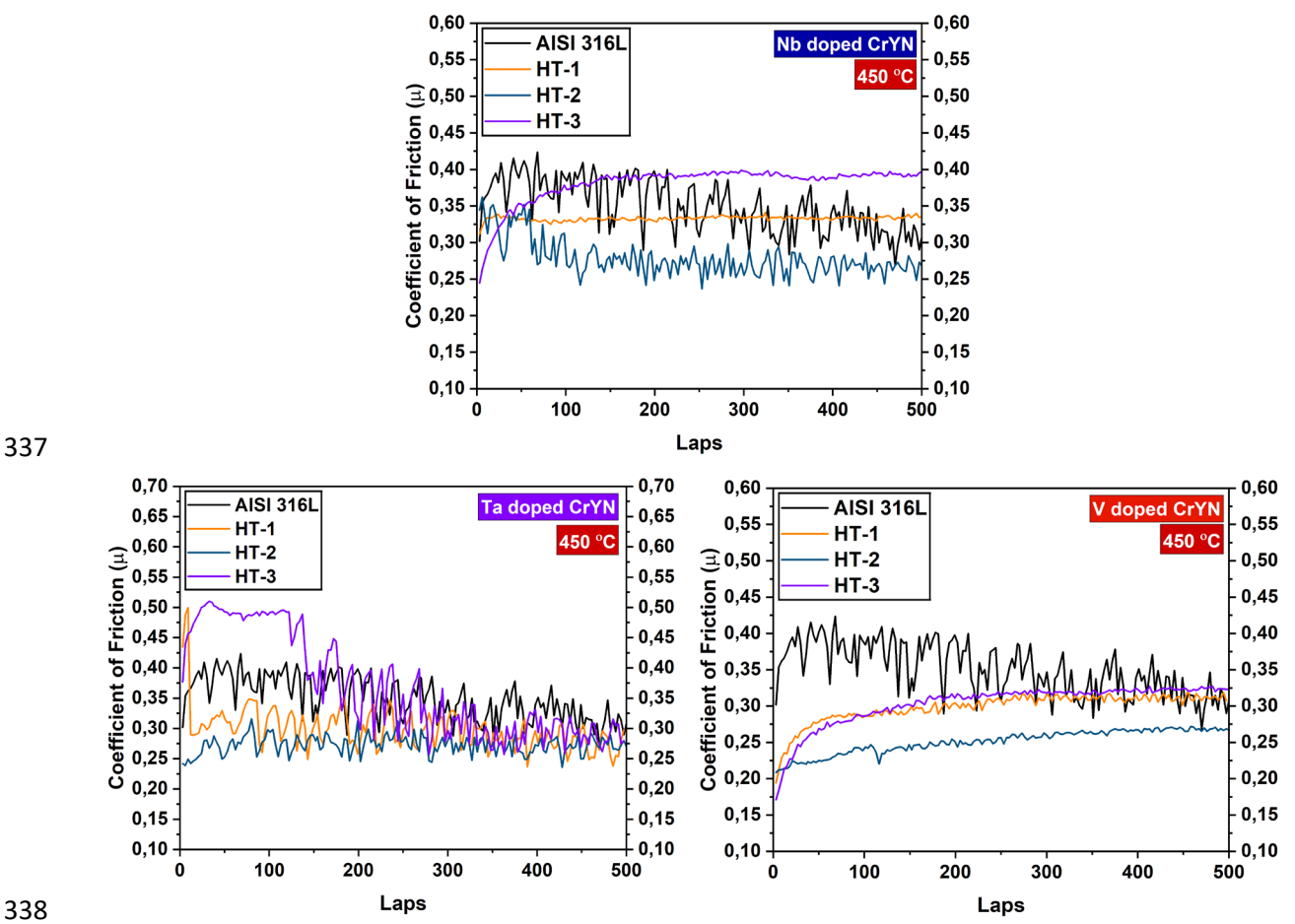


Fig. 13. Coefficient of friction (CoF) values of Nb-, Ta-, and V-doped CrYN coatings annealed at 450 °C

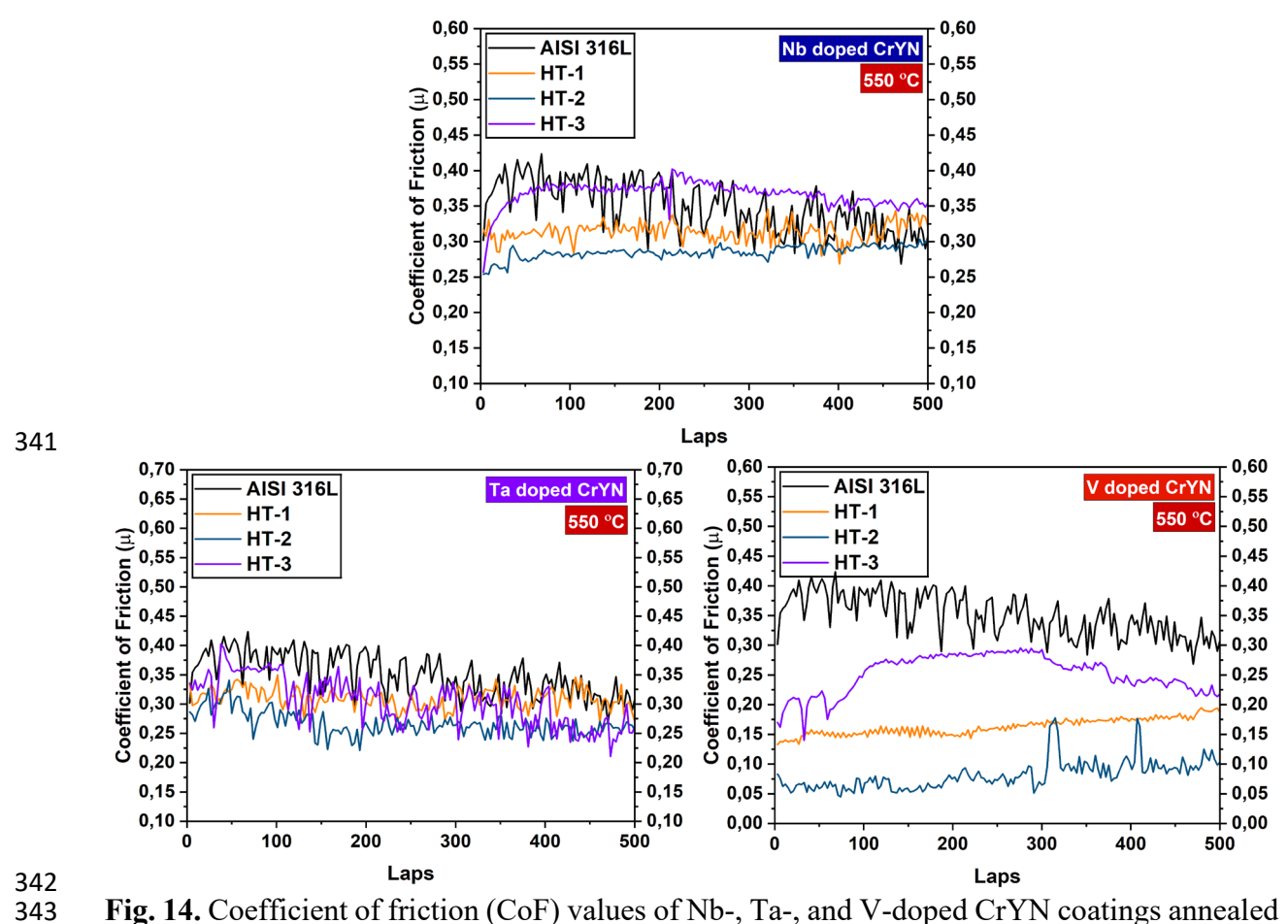
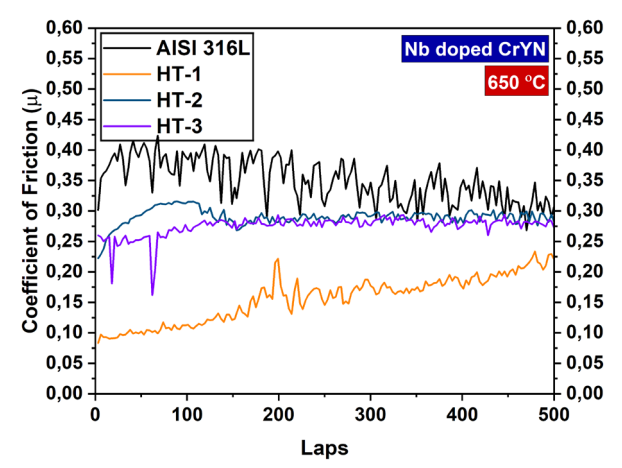


Fig. 14. Coefficient of friction (CoF) values of Nb-, Ta-, and V-doped CrYN coatings annealed at 550 °C



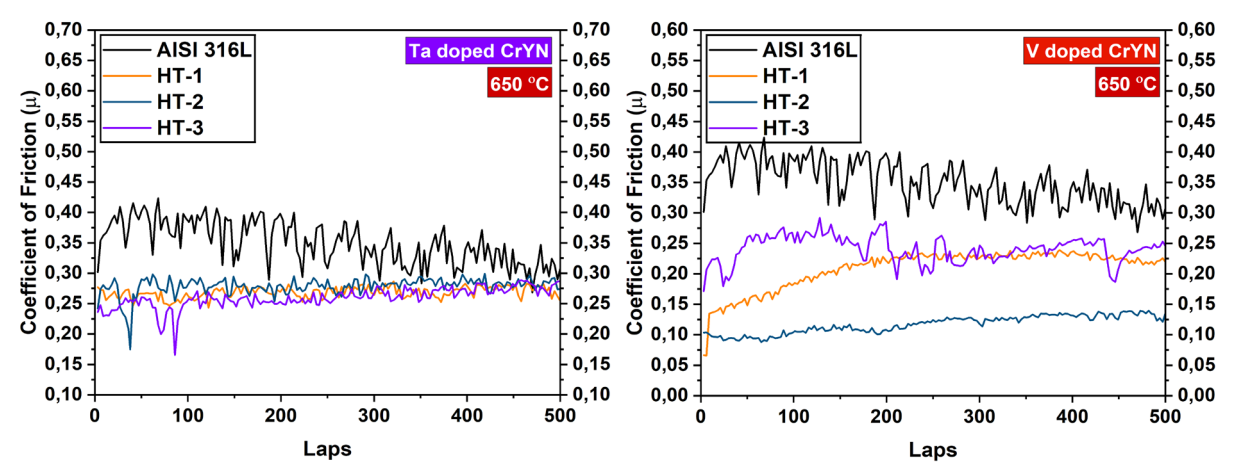


Fig. 15. Coefficient of friction (CoF) values of Nb-, Ta-, and V-doped CrYN coatings annealed at 550 °C

To provide a baseline for comparison, uncoated AISI 316L substrates were also subjected to high-temperature tribological testing at 450 °C, 550 °C, and 650 °C. As shown in Fig. 16, the wear scars on the substrates and corresponding wear tracks on the Al₂O₃ counterface exhibit severe delamination, furrow formation, and substantial debris generation across all temperatures, indicating pronounced adhesive and abrasive wear mechanisms in the absence of protective coatings.

For Nb-doped coatings, post-annealing wear tracks appeared smoother with fewer furrows, especially in HT-1 and HT-2 (Fig. 17). The dominant wear mechanism was cohesive failure, with little or no delamination, and minimal debris was observed on the pin surface. This supports the observed decrease in friction and implies improved structural stability at elevated temperatures. In Ta-doped coatings, some furrow formation was still present, but signs of delamination or edge damage were less severe after annealing (Fig. 18). The coatings maintained cohesive wear behavior with stable friction performance. V-doped coatings showed the most distinct wear patterns. At 450 °C and 550 °C, significant delamination and debris accumulation was observed (Fig. 19), which coincided with increased friction. However, at 650 °C, the wear tracks appeared smoother and debris was reduced, indicating improved wear resistance. This improvement may be due to microstructural changes or densification at higher temperatures. Overall, the wear scar and pin surface images (Figs. 17–19) indicate that thermal treatments enhance the tribological performance of CrYN coatings, especially in Nb- and Ta-doped types, by contributing to more stable surface conditions. In V-doped coatings, notable improvements were only evident after the highest temperature treatment.



Fig. 16. Wear scars on AISI 316L substrate and the corresponding wear tracks on Al₂O₃ pins after annealing at 450 °C, 550 °C, and 650 °C.

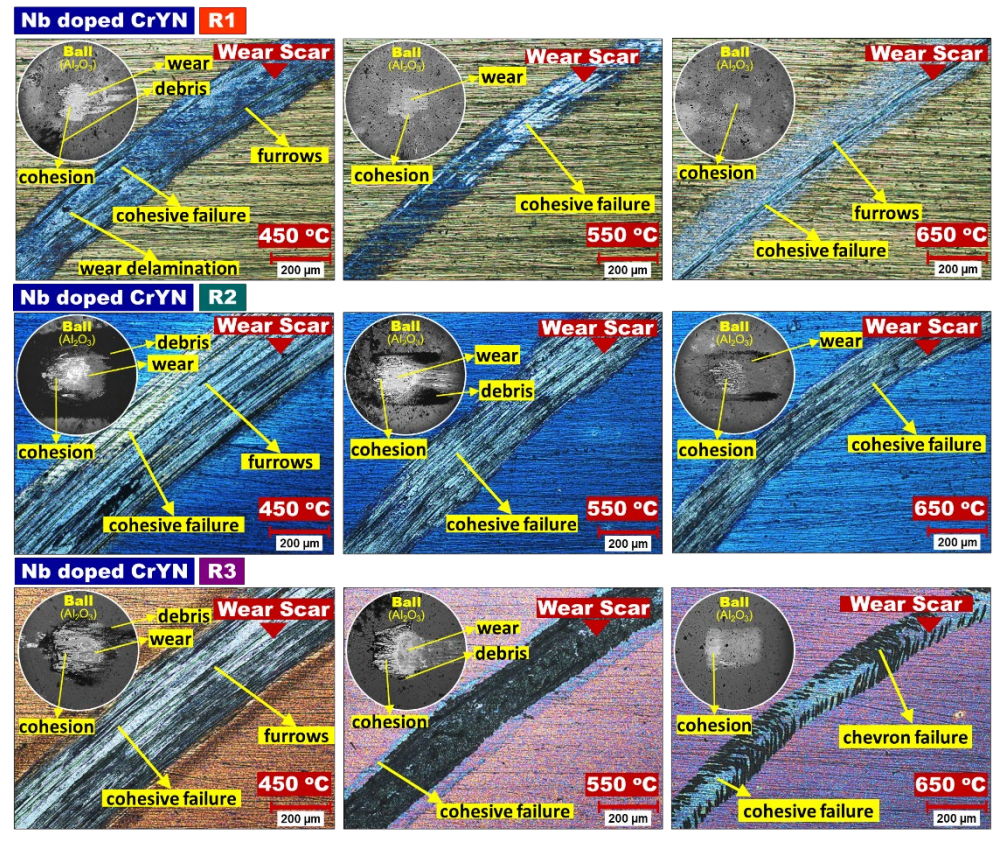


Fig. 17. Wear scars on Nb-doped CrYN coatings and the corresponding wear tracks on Al₂O₃ pins after annealing at 450 °C, 550 °C, and 650 °C.



Fig. 18. Wear scars on Ta-doped CrYN coatings and the corresponding wear tracks on Al₂O₃ pins after annealing at 450 °C, 550 °C, and 650 °C.



Fig. 19. Wear scars on V-doped CrYN coatings and the corresponding wear tracks on Al₂O₃ pins after annealing at 450 °C, 550 °C, and 650 °C.

4. Conclusion

382

- 383 This study systematically investigated the high-temperature tribological and adhesion behavior
- of Nb-, Ta-, and V-doped CrYN coatings deposited on AISI 316L stainless steel substrates
- using closed-field unbalanced magnetron sputtering. The coating parameters were selected
- from previous Taguchi L9 optimization studies and further assessed at elevated temperatures
- of 450 °C, 550 °C, and 650 °C. The main findings are summarized as follows:
- 1. High-temperature tribological tests revealed that Nb-doped coatings exhibited a
- reduction in friction from ~ 0.55 at room temperature to ~ 0.30 at 650 °C ($\approx 45\%$
- decrease), Ta-doped coatings maintained stable friction values (~0.40) across all
- temperatures (<5% variation), and V-doped coatings showed a distinct trend—rising
- from ~ 0.13 at room temperature to ~ 0.30 at 450 °C ($\approx 115\%$ increase), but then
- decreasing to ~ 0.10 at 550 °C and stabilizing around ~ 0.12 at 650 °C.
- 2. All coatings retained adhesion stability after annealing, with V-doped variants
- 395 exhibiting the least damage.
- 3. Hardness values ranged from 8.8 to 15.3 GPa, consistent with literature-reported CrYN
- 397 coatings.

401

406

- 4. These results confirm that Me-doped CrYN coatings, particularly V-doped variants, are
- promising candidates for high-temperature applications requiring both low friction and
- 400 reliable adhesion.

Declaration of competing interest

- 402 The authors declare that they have no known competing financial interests or personal
- relationships that could have appeared to influence the work reported in this paper.

404 Data availability

Data will be made available on request.

Acknowledgements

- This research was supported by Royal Society Projects (Grant Agreement No: IES\R2\202084)
- and Atatürk University-BAP (Grant Agreement No: FDA-2022-11399). The authors would like
- 409 to thank to Royal Society and Atatürk University for funding the project.

410 References

- 411 [1] S. Alvi, K. Saeidi, F. Akhtar, High temperature tribology and wear of selective laser 412 melted (SLM) 316L stainless steel, Wear 448–449 (2020).
- 413 https://doi.org/10.1016/j.wear.2020.203228.
- 414 [2] A.F. Yetim, H. Tekdir, K. Turalioglu, M. Taftali, T. Yetim, Tribological behavior of plasma-sprayed Yttria-stabilized zirconia thermal barrier coatings on 316L stainless steel under high-temperature conditions, Mater Lett 336 (2023). https://doi.org/10.1016/j.matlet.2023.133873.
- 418 [3] X.Q. Cao, R. Vassen, D. Stoever, Ceramic materials for thermal barrier coatings, J Eur Ceram Soc 24 (2004) 1–10. https://doi.org/10.1016/S0955-2219(03)00129-8.
- 420 [4] Y. Chen, S. Wang, Y. Hao, J. Pu, X. Jiang, L.F. Huang, L. Wang, Friction and Wear 421 Behavior of CrN Coating on 316L Stainless Steel in Liquid Sodium at Elevated 422 Temperature, Tribol Int 143 (2020). https://doi.org/10.1016/j.triboint.2019.106079.
- 423 [5] A. Bekmurzayeva, W.J. Duncanson, H.S. Azevedo, D. Kanayeva, Surface modification of stainless steel for biomedical applications: Revisiting a century-old material, Materials Science and Engineering C 93 (2018) 1073–1089. https://doi.org/10.1016/j.msec.2018.08.049.
- R.A. Antunes, A.C.D. Rodas, N.B. Lima, O.Z. Higa, I. Costa, Study of the corrosion resistance and in vitro biocompatibility of PVD TiCN-coated AISI 316L austenitic stainless steel for orthopedic applications, Surf Coat Technol 205 (2010) 2074–2081. https://doi.org/10.1016/j.surfcoat.2010.08.101.
- C.S. Oon, S.N. Kazi, M.A. Hakimin, A.H. Abdelrazek, A.R. Mallah, F.W. Low, S.K. Tiong, I.A. Badruddin, S. Kamanger, Heat transfer and fouling deposition investigation on the titanium coated heat exchanger surface, Powder Technol 373 (2020) 671–680. https://doi.org/10.1016/j.powtec.2020.07.010.
- E.D. Kozłowska, M. Szkodo, T. Muszyński, P. Adamska, The Laser Processing of the Stainless-Steel Surface Layer of a Heat Exchanger Membrane in Order to Enhance Its Heat Transfer Coefficient, Coatings 15 (2025). https://doi.org/10.3390/coatings15010072.
- M.M. Al-Asadi, H.A. Al-Tameemi, A review of tribological properties and deposition methods for selected hard protective coatings, Tribol Int 176 (2022). https://doi.org/10.1016/j.triboint.2022.107919.
- 442 [10] Y. Ren, J. Jia, X. Cao, G. Zhang, Q. Ding, Effect of Ag contents on the microstructure 443 and tribological behaviors of NbN–Ag coatings at elevated temperatures, Vacuum 204 444 (2022). https://doi.org/10.1016/j.vacuum.2022.111330.
- 445 [11] A. Keleş, H. Çiçek, Ö. Baran, Y. Totik, İ. Efeoğlu, Determining the critical loads of V 446 and Nb doped ternary TiN-based coatings deposited using CFUBMS on steels, Surf Coat 447 Technol 332 (2017) 168–173. https://doi.org/10.1016/j.surfcoat.2017.07.085.

- 448 [12] Y.I. Chen, K.Y. Lin, C.C. Chou, Thermal stability of CrTaN hard coatings prepared 449 using biased direct current sputter deposition, in: Thin Solid Films, Elsevier B.V., 2013: 450 pp. 606–611. https://doi.org/10.1016/j.tsf.2012.11.047.
- 451 [13] X. Li, W. Wu, H. Dong, Microstructural characterisation of carbon doped CrAlTiN nanoscale multilayer coatings, Surf Coat Technol 205 (2011) 3251–3259. https://doi.org/10.1016/j.surfcoat.2010.11.046.
- 454 [14] M. Fenker, M. Balzer, H. Kappl, Corrosion protection with hard coatings on steel: Past approaches and current research efforts, Surf Coat Technol 257 (2014) 182–205. 456 https://doi.org/10.1016/j.surfcoat.2014.08.069.
- M. Ghufran, G.M. Uddin, S.M. Arafat, M. Jawad, A. Rehman, Development and tribo-457 mechanical properties of functional ternary nitride coatings: Applications-based 458 comprehensive review, Proceedings of the Institution of Mechanical Engineers, Part J: 459 Journal Engineering Tribology (2021)196-232. 460 of 235 https://doi.org/10.1177/1350650120933412. 461
- 462 [16] J. Zhang, Z. Li, Y. Wang, S. Zhou, Y. Wang, Z. Zeng, J. Li, A new method to improve 463 the tribological performance of metal nitride coating: A case study for CrN coating, 464 Vacuum 173 (2020). https://doi.org/10.1016/j.vacuum.2019.109158.
- 465 [17] Y.C. Chim, X.Z. Ding, X.T. Zeng, S. Zhang, Oxidation resistance of TiN, CrN, TiAlN and CrAlN coatings deposited by lateral rotating cathode arc, Thin Solid Films 517 (2009) 4845–4849. https://doi.org/10.1016/j.tsf.2009.03.038.
- D. Wang, M. Hu, D. Jiang, Y. Fu, Q. Wang, J. Yang, J. Sun, L. Weng, The improved corrosion resistance of sputtered CrN thin films with Cr-ion bombardment layer by layer, Vacuum 143 (2017) 329–335. https://doi.org/10.1016/j.vacuum.2017.06.040.
- [19] G. Gulten, B. Yaylali, I. Efeoglu, Y. Totik, P. Kelly, J. Kulczyk-Malecka, Effect of Nb and V doped elements on the mechanical and tribological properties of CrYN coatings,
 Surf Coat Technol 477 (2024). https://doi.org/10.1016/j.surfcoat.2023.130297.
- 474 [20] B. Yaylali, G. Gulten, I. Efeoglu, Y. Totik, P. Kelly, J. Kulczyk-Malecka, Influence of 475 Nb and Ta on the corrosion and mechanical properties of CrYN coatings, Surf Coat 476 Technol 476 (2024). https://doi.org/10.1016/j.surfcoat.2023.130249.
- 477 [21] I. Efeoglu, G. Gülten, B. Yaylalı, Y. Totik, P. Kelly, J. Kulczyk-Malecka, Development of coatings for hostile environments, 2022.
- 479 [22] R. Schelfhout, K. Strijckmans, D. Depla, Sputter yield measurements to evaluate the 480 target state during reactive magnetron sputtering, Surf Coat Technol 399 (2020). 481 https://doi.org/10.1016/j.surfcoat.2020.126097.
- N. Mahne, M. Čekada, M. Panjan, Total and Differential Sputtering Yields Explored by SRIM Simulations, Coatings 12 (2022). https://doi.org/10.3390/coatings12101541.
- 484 [24] W. Kock, P. Paschen, Tantalum-Processing, Properties and Applications, n.d.
- 485 [25] H.A. Im, S. An, K. bong Kim, S. Yang, J. woo Lee, J.W. Jeong, Effect of co-addition of Nb/Zr on the microstructure and soft magnetic properties of Fe77.5Si11.5B7NbxZr3-

- 487 xCu1 nanocrystalline alloys, J Alloys Compd 1010 (2025). 488 https://doi.org/10.1016/j.jallcom.2024.177636.
- 489 [26] S. Grigoriev, C. Sotova, A. Metel, V. Zhylinski, F. Milovich, A. Seleznev, Y. Xue, A. Vereschaka, Wear Resistance and Failure Mode of Coatings Based on the ZrN System with the Introduction of Ti, Nb, and Hf Deposited on a Titanium Alloy Substrate, Metals (Basel) 15 (2025). https://doi.org/10.3390/met15020163.
- 493 [27] B.J. Lagerkvist, A. Oskarsson, Vanadium, Handbook on the Toxicology of Metals, Third Edition (2007) 905–923. https://doi.org/10.1016/B978-012369413-3/50101-4.
- 495 [28] A.S. Kuprin, V.D. Ovcharenko, A. Gilewicz, G.N. Tolmachova, I. V. Kolodiy, R.L. Vasilenko, T. Kuznetsova, V. Lapitskaya, B. Warcholinski, Structural, mechanical and tribological properties of Cr-V-N coatings deposited by cathodic arc evaporation, Tribol Int 165 (2022). https://doi.org/10.1016/j.triboint.2021.107246.
- 499 [29] A.M. Jabonero, A. Doutor, R. Gil, H. Serra, Deposition of Thick Nanostructured Cr-500 based Coatings by HiPIMS Deposição de revestimentos à base de Cr nanoestruturados 501 espessos por HiPIMS, n.d.
- 502 [30] P.J. Kelly, A.A. Onifade, Y. Zhou, G.C.B. Clarke, M. Audronis, J.W. Bradley, The influence of pulse frequency and duty on the deposition rate in pulsed magnetron sputtering, Plasma Processes and Polymers 4 (2007) 246–252. https://doi.org/10.1002/ppap.200600159.
- N. Nedfors, A. Mockute, J. Palisaitis, P.O.Å. Persson, L.Å. Näslund, J. Rosen, Influence of pulse frequency and bias on microstructure and mechanical properties of TiB2 coatings deposited by high power impulse magnetron sputtering, Surf Coat Technol 304 (2016) 203–210. https://doi.org/10.1016/J.SURFCOAT.2016.06.086.
- [32] Z.T. Wu, Z.B. Qi, F.P. Zhu, B. Liu, Z.C. Wang, Influences of Y Addition on Mechanical
 Properties and Oxidation Resistance of CrN Coating, Phys Procedia 50 (2013) 150–155.
 https://doi.org/10.1016/J.PHPRO.2013.11.025.
- 513 [33] D. Depla, R. De Gryse, Target poisoning during reactive magnetron sputtering: Part I: the influence of ion implantation, Surf Coat Technol 183 (2004) 184–189. https://doi.org/10.1016/J.SURFCOAT.2003.10.006.
- [34] K.P. Budna, P.H. Mayrhofer, J. Neidhardt, É. Hegedűs, I. Kovács, L. Tóth, B. Pécz, C.
 Mitterer, Effect of nitrogen-incorporation on structure, properties and performance of
 magnetron sputtered CrB2, Surf Coat Technol 202 (2008) 3088–3093.
 https://doi.org/10.1016/J.SURFCOAT.2007.11.009.
- [35] S. She, C. Wang, M. Chen, V. Ji, Mechanical Properties and Strengthening Mechanisms
 of FCC-Based and Refractory High-Entropy Alloys: A Review, Metals 2025, Vol. 15,
 Page 247 15 (2025) 247. https://doi.org/10.3390/MET15030247.
- 523 [36] Z. Lu, C. Zhang, C. Zeng, S. Ren, J. Pu, A novel design by constructing MoS2/WS2 524 multilayer film doped with tantalum toward superior friction performance in multiple 525 environment, J Mater Sci 56 (2021) 17615–17631. https://doi.org/10.1007/S10853-021-526 06217-1/FIGURES/12.

- 527 [37] C. Hu, Y.X. Xu, L. Chen, F. Pei, Y. Du, Mechanical properties, thermal stability and oxidation resistance of Ta-doped CrAlN coatings, Surf Coat Technol 368 (2019) 25–32. 529 https://doi.org/10.1016/J.SURFCOAT.2019.04.026.
- 530 [38] A.C. Karaoglanli, H. Dikici, Y. Kucuk, Effects of heat treatment on adhesion strength of 531 thermal barrier coating systems, Eng Fail Anal 32 (2013) 16–22. 532 https://doi.org/10.1016/J.ENGFAILANAL.2013.02.029.
- J.A. Lenis, F.M. Hurtado, M.A. Gómez, F.J. Bolívar, Effect of thermal treatment on structure, phase and mechanical properties of hydroxyapatite thin films grown by RF magnetron sputtering, Thin Solid Films 669 (2019) 571–578. https://doi.org/10.1016/J.TSF.2018.11.045.
- 537 [40] A. Lahmar, G.H. Lee, M. Cailler, C. Constantinescu, Adhesion studies of magnetron 538 sputtered copper films on steel substrates: Effects of heat treatments, Thin Solid Films 539 198 (1991) 115–137. https://doi.org/10.1016/0040-6090(91)90331-Q.
- [41] T.C. Lin, B.J. Jheng, H.M. Yen, W.C. Huang, Thermal Annealing Effects of V2O5 Thin
 Film as an Ionic Storage Layer for Electrochromic Application, Materials 2022, Vol. 15,
 Page 4598 15 (2022) 4598. https://doi.org/10.3390/MA15134598.
- 543 [42] A. Pawlicka, M. Atik, M.A. Aegerter, Synthesis of multicolor Nb2O5 coatings for 544 electrochromic devices, Thin Solid Films 301 (1997) 236–241. 545 https://doi.org/10.1016/S0040-6090(96)09583-1.
- 546 [43] W. Ren, G.D. Yang, A.L. Feng, R.X. Miao, J.B. Xia, Y.G. Wang, Annealing effects on 547 the optical and electrochemical properties of tantalum pentoxide films, Journal of 548 Advanced Ceramics 10 (2021) 704–713. https://doi.org/10.1007/S40145-021-0465-2.
- 549 [44] E. Lugscheider, O. Knotek, K. Bobzin, S. Bärwulf, Tribological properties, phase generation and high temperature phase stability of tungsten- and vanadium-oxides deposited by reactive MSIP-PVD process for innovative lubrication applications, Surf Coat Technol 133–134 (2000) 362–368. https://doi.org/10.1016/S0257-8972(00)00963-553
- 554 [45] R. Franz, C. Mitterer, Vanadium containing self-adaptive low-friction hard coatings for high-temperature applications: A review, Surf Coat Technol 228 (2013) 1–13. https://doi.org/10.1016/J.SURFCOAT.2013.04.034.
- 557 [46] R. Kumar, I. Hussainova, R. Rahmani, M. Antonov, Solid Lubrication at High-558 Temperatures—A Review, Materials 2022, Vol. 15, Page 1695 15 (2022) 1695. 559 https://doi.org/10.3390/MA15051695.
- [47] R. Franz, J. Neidhardt, B. Sartory, R. Kaindl, R. Tessadri, P. Polcik, V.H. Derflinger, C.
 Mitterer, High-temperature low-friction properties of vanadium-alloyed AlCrN coatings,
 Tribol Lett 23 (2006) 101–107. https://doi.org/10.1007/S11249-006-9064 1/FIGURES/8.